Square Patterns in Bénard-Marangoni Convection

Michael Bestehorn

Institut für Theoretische Physik und Synergetik, Universität Stuttgart,
Pfaffenwaldring 57/4, 70550 Stuttgart, Germany
(Received 12 June 1995)

The evidence of square patterns in Bénard-Marangoni convection relatively far above threshold is demonstrated for the first time by means of a direct numerical integration of the three-dimensional Navier-Stokes equations. It is shown that regular squares are only obtained for a finite Prandtl number. Finally a qualitative explanation of the obtained sequence of instabilities based on a model of amplitude equations is discussed.

If a fluid layer with a free upper surface is heated from below convection usually emerges in the form of regular hexagonal patterns. This is known as Bénard-Marangoni convection (BMC) [1–5]. It is known from experiments that, if the externally applied temperature gradient is increased far above the threshold of convection, the hexagons get more and more disordered and defects built up of hexagon-pentagon pairs occur [6]. Recently, it was shown experimentally by Nitschke and Thess [7] that a fluid unstable to BMC may form also a completely regular square pattern bifurcating from hexagons as a secondary instability (Fig. 1).

Direct numerical simulations:—In the first part of this Letter we wish to present numerical results from a direct solution of the Navier-Stokes equations and the temperature equation for an incompressible fluid with finite Pr. We solved the coupled equations for the dimensionless toroidal and poloidal part ψ and ϕ of the velocity field (e.g., [8]):

$$\left\{\Delta - \frac{1}{\text{Pr}}\,\partial_t\right\}\Delta\Delta_2\psi = -\frac{1}{\text{Pr}}\{\boldsymbol{\nabla} \times \boldsymbol{\nabla} \times (\tilde{\mathbf{v}} \cdot \boldsymbol{\nabla}\tilde{\mathbf{v}}\}_z,$$

$$\left\{\Delta - \frac{1}{\text{Pr}}\,\partial_t\right\}\Delta_2\phi = -\frac{1}{\text{Pr}}\{\boldsymbol{\nabla} \times (\tilde{\mathbf{v}} \cdot \boldsymbol{\nabla}\tilde{\mathbf{v}}\}_z, \qquad (1)$$

as well as the equation for the dimensionless deviations of the linear basic temperature profile

$$\{\Delta - \partial_t\}\Theta = \Delta_2\psi + \tilde{\mathbf{v}} \cdot \boldsymbol{\nabla}\Theta \qquad (2)$$

with the Prandtl number $\text{Pr} = \nu/\kappa$ being the ratio between viscosity and thermal conductivity and the horizontal Laplacian $\Delta_2 = \partial_{xx} + \partial_{yy}$. Then temperature T and velocity $\mathbf{v}$ of the fluid are given as

$$T(\mathbf{r}, t) = T_0 + (T_1 - T_0)[z + \Theta(\mathbf{r}, t)],$$

$$\tilde{\mathbf{v}}(\mathbf{r}, t) = \boldsymbol{\nabla} \times \{\phi(\mathbf{r}, t)\mathbf{z}_0\} + \boldsymbol{\nabla} \times \boldsymbol{\nabla} \times \{\psi(\mathbf{r}, t)\mathbf{z}_0\}, \quad (3)$$

$$\mathbf{v} = \frac{\kappa}{d}\,\tilde{\mathbf{v}},$$

where T_0 and T_1 are the temperatures on the lower and upper surfaces of the fluid, respectively, in the state without convection, $\mathbf{z}_0$ is the unit vector in the vertical direction, and d is the height of the layer. On the free upper surface a coupling between temperature and velocity is established by the surface tension of the fluid (e.g., [9]) for $z = 1$:

$$\psi = 0, \quad \partial_z\phi = 0, \quad \partial_z^2\psi = -M\Theta, \quad \partial_z\Theta = -\text{Bi}\Theta,$$
$$(4)$$

where M denotes the Marangoni number and is proportional to the dependence of the surface tension on temperature γ as well as to the externally applied temperature difference $T_1 - T_0$:

$$M = \frac{\gamma(T_1 - T_0)d}{\rho\nu\kappa}. \qquad (5)$$

The Biot number Bi was fixed to $\text{Bi} = 0.1$, reflecting the much lower thermal conductivity of the air compared to that of the silicon oil. On the bottom ($z = 0$), we assume the usual rigid boundary conditions (BC's)

$$\Theta(\mathbf{r}) = \phi(\mathbf{r}) = \psi(\mathbf{r}) = \partial_z\psi(\mathbf{r}) = 0. \qquad (6)$$

A linear stability analysis of (1) and (2) with (4) and (6) shows that the motionless state loses stability and
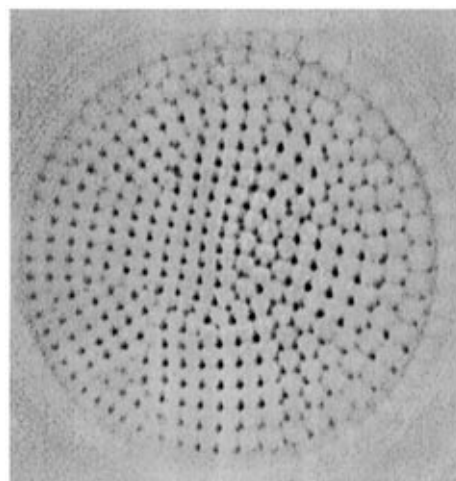

FIG. 1. Squares obtained experimentally by Nitschke and Thess at $\varepsilon = 3.2$. The fluid they used was silicon oil with a viscosity of 10 centistokes, corresponding to $\text{Pr} = 100$. In the dark areas, the fluid is colder and descends.

convection sets in at $M_c \approx 80$ in the form of spatially periodic patterns with wave vector $|\mathbf{k}_c| \approx 2$ (see, e.g., [9,10]). To solve the full nonlinear problem, we used an extension of the algorithm described in detail in [5] to the case of a finite Pr. In the two lateral directions we assume periodic BC. With our code we are able to describe pattern formation for relatively large values of the reduced control parameter $\varepsilon = (M - M_c)/M_c$ up to $\varepsilon = 5$. Figure 2(a) shows a stable solution for $\varepsilon = 3$ and large Pr = 10 000 that was achieved after $300 t_v$ ($t_v = d^2/\kappa$ is the vertical diffusion time of heat). The structure resembles very much those obtained experimentally by Cerisier *et al.* [11] and contains mainly pentagons and deformed hexagons (in [6] the working fluid was a silicon oil with Pr = 880). The situation changes if Pr is decreased to smaller, but still large values. Figure 2(b) shows a stable structure for Pr = 500 and $\varepsilon = 3$. The pattern is now more ordered and shows larger regions of regular squares. For still smaller Pr = 50 we found an even more regular structure of squares [Fig. 2(c)]. If we decrease the heating to $\varepsilon = 1$ the typical hexagons are reconstructed for all Pr in a very short time of about $5 t_v$. This is in agreement with [7]. Nitschke and Thess determined the transition from squares to rolls at $\varepsilon = 2.35 \pm 0.4$ for Pr = 100. In Fig. 3 we used a modified Wigner-Seitz method (e.g., [12,13]) to construct the elementary cells around the maxima of the temperature fields at the free surface shown in Fig. 2. Obviously the number of squares (here colored black) increases significantly with decreasing Pr.

From the above mentioned results one may deduce the following picture: Near the threshold of convection regular hexagons are formed. For larger values of ε the tendency for the stabilization of squares increases and a *stationary* "mixed state" of squares and hexagons is reached, dominated by many defects, deformed hexagons, and penta-hepta defects as shown in Fig. 2(a). The vertical vorticity Φ that is of order 1/Pr and which is always present for a finite Pr seems to act as a "lubricant" and may help to "soften" the structure. Its inclusion

leads to a destabilization of the disordered states as in Fig. 2(a) and catalyzes a further transient until a more or less regular square pattern is reached, where eventually only a few defects can survive. It is supposed [7] that this transient is mediated by pentagons. The pentagons are not equilateral but have a smallest side that slowly vanishes during the transient phase, leaving finally a square. The time scale on which this ordering effect takes place is proportional to Pr, just as the relaxation of the vertical vorticity. If Pr is decreased further, the ordering effect gets stronger and the time in which the formation and stabilization of regular squares takes place becomes shorter (Fig. 4).

Amplitude equations:—Hexagons and rolls as well as the hysteretic transition between them can be described in the frame of amplitude equations, as shown by numerous authors (for a review, see, e.g., [14,15], and references therein). It is well known that the quadratic terms in the amplitudes account for the formation of hexagons [16], whereas the cubic nonlinearities may select either rolls or squares, depending on the value of the cross coupling term between perpendicular rolls [17]. To be more specific we discuss the following model:

$$\dot{\xi}_1 = \tilde{\varepsilon}\xi_1 + A\xi_2\xi_3$$
$$\quad - \xi_1(B_0\xi_1^2 + B_{60}\xi_2^2 + B_{60}\xi_3^2 + B_{90}\xi_4^2),$$
$$\dot{\xi}_2 = \tilde{\varepsilon}\xi_2 + A\xi_1\xi_3$$
$$\quad - \xi_2(B_0\xi_2^2 + B_{60}\xi_1^2 + B_{60}\xi_3^2 + B_{30}\xi_4^2),$$
$$\dot{\xi}_3 = \tilde{\varepsilon}\xi_3 + A\xi_1\xi_2$$
$$\quad - \xi_3(B_0\xi_3^2 + B_{60}\xi_1^2 + B_{60}\xi_2^2 + B_{30}\xi_4^2),$$
$$\dot{\xi}_4 = \tilde{\varepsilon}\xi_4 - \xi_4(B_0\xi_4^2 + B_{30}\xi_2^2 + B_{30}\xi_3^2 + B_{90}\xi_1^2),$$
$$\tag{7}$$

and $\varepsilon \propto \tilde{\varepsilon}$. Here ξ_i are amplitudes of plane waves with wave vectors $\mathbf{k}_i$, where $\mathbf{k}_i = |\mathbf{k}_c|$, $\sum_{i=1}^{3}\mathbf{k}_i = 0$, and $\mathbf{k}_4$ is perpendicular to $\mathbf{k}_1$. The four equations (7) contain the solution rolls ($\xi_1 \neq 0$, $\xi_i = 0$, $i > 1$), hexagons ($\xi_1 = \xi_2 = \xi_3 \neq 0$, $\xi_4 = 0$), and squares ($\xi_1 = \xi_4 \neq 0$, $\xi_2 = \xi_3 = 0$) as fixed points. The stability of these
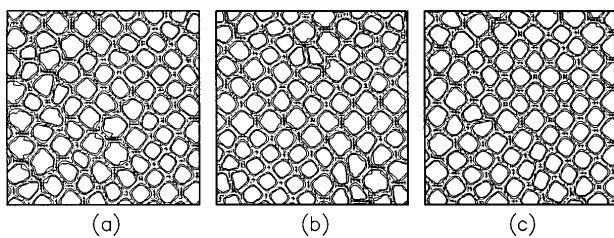

FIG. 2. Contour lines of the temperature at the surface of the fluid far above threshold $\varepsilon = 3$. Starting from a randomly distributed initial condition, the numerical integration of (1) was carried out for three different values of Pr until $t = 300 t_v$ was reached. All patterns were then stationary. With a decreasing Prandtl number, the tendency to form regular squares increases. (a) Pr = 10 000, (b) Pr=500, (c) Pr = 50.
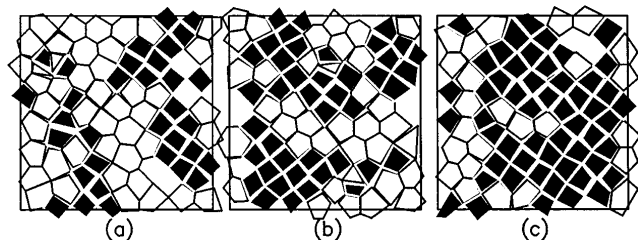

FIG. 3. Wigner-Seitz cells defined by the maxima of the fields shown in Fig. 2. The contribution of squares (S), pentagons (P), and hexagons (H) in percent is for (a) Pr = 10 000: 40% S, 45% P, 6% H, (b) Pr = 500: 45% S, 40% P, 5% H, (c) Pr = 50: 52% S, 37% P, 5% H.
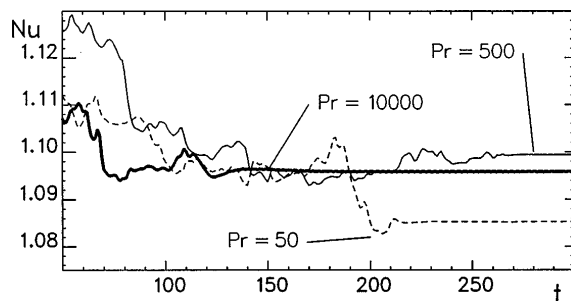
FIG. 4. Nusselt number measuring the vertical heat flux through the fluid layer for the different runs leading to the final states shown in Fig. 2. The patterns are stationary when Nu reaches a constant value. For very large (or infinite) Pr, pattern formation ends in a rather disordered state after a short time. For smaller Pr, the states get more and more ordered and may overcome many of the defects on a time scale $\propto$ Pr.

solutions depends on the values of the coefficients. In a previous work [18] we showed by a numerical calculation of the coefficients A, B_0, and B_{60} that for BMC always $A, B_0, B_{60} > 0$ and $B_0 < B_{60}$. Moreover, we found that $B_0 < B_{90}$ so squares should never be stable and the transition goes from hexagons to rolls if ε is increased. On the other hand, using amplitude equations one usually computes the coefficients at the critical point $\varepsilon = 0$. This may explain also the relatively small value found by other authors [19,20] of $\varepsilon_2 \approx 1.8$, where hexagons finally lose their stability and should give way to rolls [in [18] we found $\varepsilon_2 \approx 0.9$ (Bi = 0), a value which later turned out to be erroneous by a factor of 2]. However, in all experiments on BMC, rolls were never obtained and hexagons were stable for much larger values of ε [6,21]. A sequence of instabilities that is qualitatively similar to that obtained in experiments is found if we allow the cubic coefficients to depend weakly on ε. It is sufficient if only B_0 is assumed to vary linearly:

$$B_0 = b_0 + \beta_0 \tilde{\varepsilon}. \qquad (8)$$

We mention that this assumption is completely heuristic and will lead to a model that describes the numerically found sequence of instabilities qualitatively. In fact, all the coefficients in (7) depend on ε; however, we do not claim to derive them from the basic equations (1) far above threshold. A more systematic approach should at least include amplitude equations for the modes with positive eigenvalues. We note also that (8) leads to a higher order expression in ε then the usual cubic terms. Then it could be important to include at least quartic terms in the amplitudes (due to symmetry reasons they would not change the stability of squares, but that of hexagons). Also the question of validity of (7) may be asked so far above threshold. For a pitchfork bifurcation ($A = 0$) the amplitudes may be expanded and are of $O(\sqrt{\varepsilon})$. On the other hand, if $A \neq 0$, and, moreover, A is not of $O(\sqrt{\varepsilon})$, which is always the case for BMC, a proper ε expansion

of the amplitudes is no longer possible. In this sense, all the amplitude equations derived for BMC and discussed in the literature (e.g., [6,16,18–20]) are not systematic in ε. Under these restrictions we continue considering (7) with (8) as a model. If we chose $\beta_0 > 0$, a scenario as shown in Fig. 5 is found. For large enough A, a transition from hexagons to squares is now possible, and the region of rolls can no longer be reached. In the phase diagram exist large regions of bistability of rolls and hexagons, or squares and hexagons, here denoted as RH,HR or SH,HS, respectively. The pattern that finally emerges in such a region corresponds to a global minimum of the potential

$$V(\xi_i) = -\frac{1}{2}\left[\tilde{\varepsilon} \sum_{i=1}^{4} \xi_i^2 + 2A\xi_1\xi_2\xi_3 - \frac{B_0}{2}\sum_{i=1}^{4}\xi_i^4 \right.$$
$$- B_{60}(\xi_1^2\xi_2^2 + \xi_1^2\xi_3^2 + \xi_2^2\xi_3^2)$$
$$\left. - \xi_4^2(B_{90}\xi_1^2 + B_{30}\xi_2^2 + B_{30}\xi_3^2) \right] \qquad (9)$$

from which (7) can be obtained by variation of ξ_i. If (9) reaches only a local minimum and if the amplitudes may depend on the spatial coordinates, small disturbances may lead to regions where the more stable pattern (global minimum) evolves. The domain boundaries separating this region suffer a force (analog to the Peach-Köhler force in solid state physics [22]) and move in such a way that (9) will decrease further towards its global minimum. In this way the hysteretic regions in Fig. 5 vanish and shrink to the dashed line where the values of (9) are equal for the two stable pattern types [23]. We note that even in this case a small region of bistability may exist if pinning effects between such a front and the underlying small scale structures are taken into account. The front can then be trapped by a hexagon (or a roll/square) for values of the control parameters in the
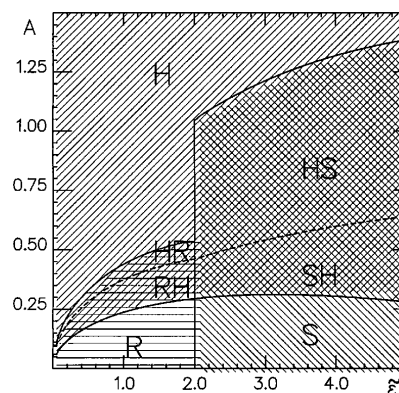

FIG. 5. Phase diagram showing the regions of different stable solutions of the model Eqs. (7) with $B_{30} = 1.8$, $B_{60} = 1.5$, $B_{90} = 1.1$, and B_0 according to (8) with $b_0 = 1$ and $\beta_0 = 0.05$. R: rolls, S: squares, H: hexagons, SH/HS: bistability of squares and hexagons, RH/HR: bistability of rolls and hexagons. The first letter in each bistable region denotes that pattern that minimizes the potential (9). On the dashed line, the potential for both pattern types is equal.

vicinity of the dashed line [23,24]. This region increases exponentially with ε. Therefore pinning effects may cause a mixed state of hexagons and squares and could explain the disordered states found experimentally as well as numerically [Fig. 2(a)] for large ε and large Pr.

For smaller values of A, the sequence hexagons–rolls–squares should be found for increasing ε. As was demonstrated recently [20,25], A depends on Pr and vanishes for $\mathrm{Pr} = 0.23c$. Indeed our numerical simulations of the Navier-Stokes equations showed for Pr close to Pr_c the transition from hexagons to rolls. If ε is increased further, the rolls get destabilized by a perpendicular set of rolls and give way to squares. However, these squares were not stable but showed an intrinsic time dependence caused by the vertical vorticity that is rather large for this small value of Pr. Of course, the vertical vorticity is not included in our amplitude model (7).

In conclusion, we may say that the experimentally as well as numerically obtained pattern transitions from hexagons to squares can be explained by the interaction of only four dominating modes or order parameters, namely, the roll amplitudes. A more complete picture could be obtained if the effects of a large scaled vertical vorticity together with spatially slowly varying amplitudes in the way outlined in [26] would be included also. The extension of (7) to more than four modes should allow us to compute the coefficients of the amplitude equations directly from the Navier-Stokes equations in a systematic way far from threshold. This could give a more quantitative picture of the experimentally and numerically observed hierarchy of instabilities. This work is currently under progress. The Prandtl number plays a key role in our observations. If Pr is very large or infinite, the structures obtained far from threshold are rather disordered. For smaller Pr, regular squares can be seen. For very small Pr we expect rolls near threshold, and for increasing ε a direct transition to squares is predicted. However, the additional degrees of freedom due to the vertical vorticity will render the patterns in the case of small Pr time depending even for small values of ε and should result in phase turbulence and a rich defect dynamics.

[1] R. A. Pearson, J. Fluid Mech. **4**, 489 (1958).
[2] E. L. Koschmieder, Adv. Chem. Phys. **26**, 177 (1974).
[3] D. A. Nield, J. Fluid Mech. **19**, 341 (1964).
[4] C. Normand, Y. Pomeau, and M. Velarde, Rev. Mod. Phys. **49**, 581 (1977).
[5] M. Bestehorn, Phys. Rev. E **48**, 3622 (1993).
[6] P. Cerisier, C. Pérez-García, and R. Occelli, Phys. Rev. E **47**, 3316 (1993).
[7] K. Nitschke and A. Thess, Phys. Rev. Lett. (to be published).
[8] F. H. Busse and R. M. Clever, J. Fluid. Mech. **91**, 319 (1979).
[9] J. K. Platten and J. C. Legros, *Convection in Liquids,* (Springer-Verlag, Berlin, 1984).
[10] C. Yih, *Fluid Mechanics* (McGraw-Hill Book Company, New York, 1969).
[11] P. Cerisier, C. Pérez-García, C. Jamond, and J. Pantaloni, Phys. Rev. A **35**, 1949 (1987).
[12] O. Madelung, *Introduction to Solid-State-Theory,* (Springer, Berlin, 1978).
[13] R. Occelli, doctoral thesis, l'Université de Provence, Marseille, France, 1985.
[14] H. Haken, *Synergetics. An Introduction* (Springer, Berlin, 1983).
[15] M. C. Cross and P. C. Hohenberg, Rev. Mod. Phys. **65**, 851 (1993).
[16] L. A. Segel, J. Fluid Mech. **21**, 345 (1965).
[17] M. R. E. Proctor, J. Fluid Mech. **113**, 469 (1981).
[18] M. Bestehorn and C. Pérez-García, Europhys. Lett. **4**, 1365 (1987).
[19] J. Bragard and G. Lebon, Europhys. Lett. **21**, 831 (1993).
[20] P. M. Parmentier, V. C. Regnier, and G. Lebon (to be published).
[21] E. L. Koschmieder and D. W. Switzer, J. Fluid Mech. **240**, 533 (1992).
[22] Y. Pomeau, S. Zaleski, and P. Manneville, Phys. Rev. A **27**, 2710 (1983).
[23] H. Herrero, C. Pérez-García, and M. Bestehorn, Chaos **4**, 15 (1994).
[24] B. Malomed, A. A. Nepomnyashchy, and M. I. Tribelsky, Phys. Rev. A **42**, 7244 (1990).
[25] A. Thess and M. Bestehorn, Phys. Rev. E (to be published).
[26] D. Siggia and A. Zippelius, Phys. Rev. Lett. **47**, 835 (1981).